Int. J. Electrochem. Sci., 10 **(2015)** 1372 - 1383

International Journal of
ELECTROCHEMICAL
SCIENCE
www.electrochemsci.org

The Role of Eliminating PEG from PEG/MCM-41 Composite on the Structural, Textural and Electrical Conductivity Properties of MCM-41

Bahaa M. Abu-Zied[1,2,*], *Mahmoud A. Hussein*[1], *and Abdullah M. Asiri*[1,2]

[1]Chemistry Department, Faculty of Science, King Abdulaziz University, P.O. Box 80203, Jeddah 21589, Saudi Arabia
[2] Center of Excellence for Advanced Materials Research (CEAMR), King Abdulaziz University, P.O. Box 80203, Jeddah 21589, Saudi Arabia
[*]E-mail: babuzaid@kau.edu.sa, babuzied@yahoo.com

Received: 28 September 2014 / *Accepted:* 17 October 2014 / *Published:* 16 December 2014

A PEG/MCM-41 composite was synthesized by a simple solution method with polyethylene glycol (PEG) and mesoporous MCM-41. The thermal behavior of the composite was studied using thermogravimetric analysis (TGA) and an *in situ* electrical conductivity measurement. The results showed that polymer degradation occurs in the temperature range of 300 to 550 °C, and is accompanied by a decrease in the electrical conductivity. Thus, to elucidate the influence of polymer elimination on the structural, textural and electrical conductivity properties of MCM-41, a sample was prepared by calcining the PEG/MCM-41 composite for 3 h at 550 °C in air. Various physico-chemical techniques such as XRD, FT-IR, FE-SEM and N_2 physisorption, were used for characterization. It was shown that the calcined solid still exhibits the mesoporous MCM-41 framework with poor ordering. A texture analysis revealed that the PEG/MCM-41 composite formation and the subsequent PEG elimination are accompanied by a loss of the type IV character of the MCM-41 and a sharp decrease in the textural parameters. The observed meso-porosity loss of the MCM-41 as a result of adding and then eliminating the PEG molecules was accompanied by a reduction of the conductivity.

Keywords: MCM-41, PEG, thermal analysis, electrical conductivity, texture properties

1. INTRODUCTION

Composite materials have recently been widely used in various fields of industrial applications due to their superior low density and cost properties. Moreover, composite materials are becoming preferable to steel due to their low specific weight and high strength [1]. Organic/inorganic composites have received wide attention in various fields of study, especially in the field of materials science to

produce new, efficient materials with excellent properties, such as low cost, low density and photoconductivity for electronics [2-4]. A huge number of applications exist for these new materials in the automotive and aerospace industries such as bushes, seals, gears, cams and shafts [5–7].

Mesoporous materials possess pores large enough (20–500 Å) to readily allow the penetration of polymer chains, resulting in better wetting and dispersion. Mesoporous silica (MS) has uniform channels with pore diameters from 2 to 50 nm, which can be used to control the size of nanoparticles during their growth. MCM-41 is considered to be the most famous mesoporous material in a family known as M41S, which was first reported by researchers of Mobil Research and Development Corporation in 1992 [8-10]. This material has received wide-spread interest for catalysts, adsorbents and membranes because of its high surface area, tunable pore size and surface chemistry via functionalization. The M41S family exhibits a hexagonal arrangement of uniform pores [10]. The incorporation of various fillers into the rubbery polymers imparts many interesting and useful properties to the particle-filled composite materials. In recent years, the effects of various types of fillers on the rubber compounds have been studied. The incorporation of MCM-41, a hexagonal member of this M41S family as a nanofiller has recently been described as an effective route for the successful preparation of nanocomposites by *in situ* supported ethylene polymerization [11,12]. These self-reinforced nanocomposites showed an increase in rigidity and an easier degradability because of the additional role of mesoporous MCM-41 as promoter for polyethylene (PE) degradation. Recently, nanomesoporous MCM-41 has been extensively studied as an effective reinforcement filler to enhance the mechanical and thermal properties of polymer materials due to its unusual characteristics, such as extended inorganic or inorganic–organic hybrid arrays with exceptional long-range ordering, highly tunable textural and large surface area properties, controlled pore size and shape [10,13]. It is expected that a polymer can either be introduced directly or produced *in situ* by polymerization of organic monomers inside the mesopores. The polymers in the nanosized pores extending along the channels to the openings cannot only enhance the miscibility through the entanglement and inter-diffusion between the matrix and the particulate but can also highly suppress the aggregation of fillers. Due to these unusual characteristics, the mesoporous MCM-41 material has recently been extensively utilized as an effective reinforcement filler to enhance the physico-chemical properties of many polymers. In this way, epoxy resin/MCM-41, polypropylene/MCM-41 and polyethylene/MCM-41 composites with enhanced thermal stability and mechanical properties have been reported [14–20].

To the best of our knowledge, there are no reports in the open literature on the effect of the removal of the organic part, which is almost a polymer matrix, from MCM-41/polymer composites on the structural, textural and electrical properties of mesoporous MCM-41. Accordingly, the present investigation seeks to elucidate the influence of eliminating the PEG molecules via calcination at 550 °C on the structural, textural and the electrical properties of MCM-41. The elimination of PEG from the PEG/MCM-41 composite was followed by thermogravimetric analysis (TGA) and in situ electrical conductivity measurements. Sample characterization was performed using X-ray diffraction (XRD), Fourier transform infrared spectroscopy (FT-IR), nitrogen adsorption at –196 °C, field emission scanning electron microscopy (FE-SEM) and electrical conductivity measurements.

2. EXPERIMENTAL

2.1 Materials

Polyethylene glycol (PEG) with an average molecular weight of 6000 and cetyl-trimethylammonium bromide (CTAB) were purchased from Aldrich Chemical Co. Tetraethylorthosilicate (TEOS) and ethyl acetate were obtained from (Merck). Ethyl alcohol (> 99.8 %) and ammonia (28 wt. %) were purchased from Prolabo. All chemicals were used without further purification.

2.2 Preparation of mesoporous MCM-41

The parent MCM-41 material was prepared according a procedure similar to that reported by Grün et al. [21]. Briefly, 2.5 g of CTAB was dissolved in 50 g of distilled water, and then 13.5 g of aqueous ammonia and 60 g of absolute ethanol were added to the surfactant solution. The solution obtained was stirred for 15 min (500 rpm) followed by the addition of 4.7 g of TEOS, which resulted in gel formation. The obtained gel was stirred for 2 h and aged for another 2 h at room temperature, and then it was filtered and washed with 300 ml of distilled water. After drying overnight at 90 °C, the sample was heated to 550 °C in air flow and kept at that temperature for 3 h to remove the template, after which it was cooled to room temperature.

2.2 PEG/MCM-41composite preparation

The PEG/MCM-41 composite containing 25 % MCM-41 was prepared using a simple solution method, as reported in our recent study [22]. Briefly, 1 g of polyethylene glycol and the MCM-41 mixture were added to 30 ml of ethyl acetate under magnetic stirring at 600 rpm at 60 °C for 8 h. This was followed by solvent evaporation in Petri dishes for at least 24 h at room temperature and under vacuum for 4 h (between 5 and 10 Torr).

2.3 Instrumentation

The TGA and DTG curves were recorded with the aid of TA (model TGA-Q500) instrument using a heating rate of 7 °C min^{-1} in nitrogen flow (40 ml min^{-1}). Powder X-ray diffractograms were obtained at 2θ values from 2° to 80° with the aid of a PANalytical (X'pert PRO, Holland) instrument with a Ni-filtered Cu Kα radiation source (λ = 0.15418 nm) operated at 45 kV, 40 mA and a step of 0.02° s^{-1}. FT-IR spectra were recorded over the wavenumber range of 4000 to 400 cm^{-1} with the aid of a Thermo-Nicolet iS50 FT-IR spectrometer using an attenuated Total Reflectance (ATR) sampling accessory. Adsorption-desorption isotherms of nitrogen (at –196 °C) were conducted using a Quantachrome (Nova 3200 series) multi-gas adsorption apparatus. Scanning electron micrographs were obtained using a JEOL (model JSM-7600F) field-emission scanning electron microscope (FE-SEM). DC electrical conductivity measurements were performed using a Pyrex glass cell operated up

to 500 °C. The resistance measurements were conducted using a Keithley 610C solid-state electrometer. In each run 0.5 g of the sample was placed between two silver electrodes (1.0-cm diameter) and pressed by the upper electrode to ensure good contact between the particles. The temperature was controlled with a WEMA temperature controller.

3. RESULTS AND DISCUSSION

3.1 Thermal analysis and in situ electrical conductivity measurements

The thermal behavior of the PEG/MCM-41 composite was tested using TGA analysis. Fig. 1 shows the obtained normalized weight loss (NWL) and its derivative in a dynamic atmosphere of nitrogen at a heating rate of 7 °C min^{-1}. NWL = 100 × [(w − w_{MCM-41})/(w_{init} − w_{MCM-41})], where w, w_{MCM-41}, and w_{init} represent the weight of the sample at temperature T, the weight of MCM-41 loaded, and the initial weight of the polymer, respectively. Four weight-loss (WL) steps could be observed upon heating the PEG/MCM-41 composite up to 800 °C.

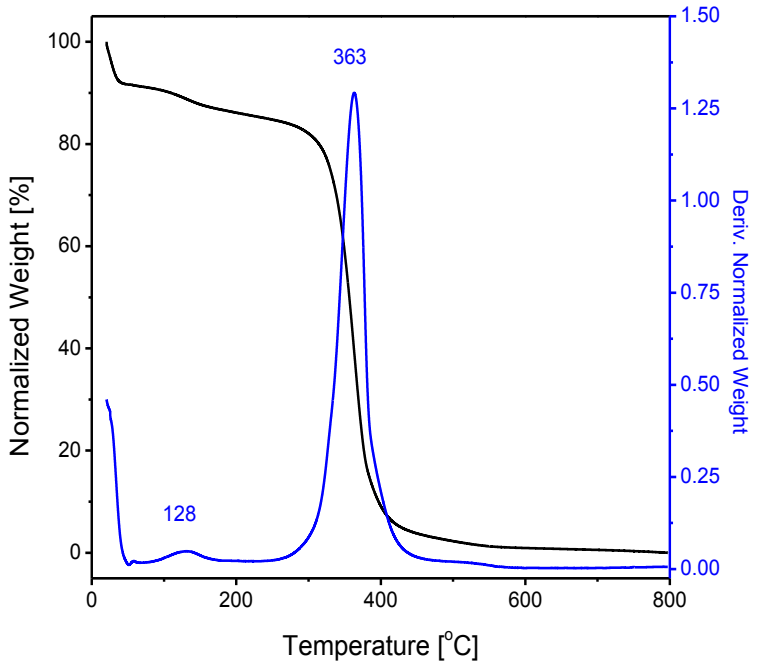

Figure 1. TGA and DTG curves obtained for the MCM-41/PEG (25 wt. %) composite.

The first step extends from ambient until approximately 55 °C, and corresponds to the removal of adsorbed water. The second WL, which is maximized at 128 °C, could be attributed to the elimination of water molecules from the MCM-41 pores. The third WL step is steep and is maximized at 363 °C. This step is most likely related to the decomposition of the PEG molecules [22,23]. The final WL step extends over the temperature range of ~ 420 to 550 °C. This step may be related to a

slow evolution of the non-volatile carbonaceous residues formed at the end of the main decomposition step of PEG [22,23].

In situ electrical conductivity measurements represent an interesting tool to recognize the various stages of the decomposition of solids [23–25]. The combination of this tool with thermogravimetric analysis gives much greater insight into the decomposition processes. The temperature dependence of log σ, measured in nitrogen atmosphere up to 510 °C (the temperature limit of our conductivity cell) is shown in Fig. 2. The obtained plot can be divided into five regions (a–e). In the first region, extends from ambient until 110 °C, the conductivity increases with increasing temperature. In the second region, 110-165 °C, the conductivity shows a slight plateau followed by another increase. In region (c), extending from 165 to 300 °C, a mild conductivity increase can be observed. Raising the heating temperature till 510 °C is accompanied by the emergence of two minima at 370 and 477 °C as shown in regions (d) and (e), respectively. Bearing in mind the information inferred from the TGA analysis, the conductivity changes observed in regions (a) and (b) can be related to the removal of water molecules from the PEG/MCM-41 composite. The steep ln σ decrease observed in region (d) can be correlated with the PEG decomposition, which is maximized at 363 °C (Fig. 1). Finally, it is reasonable to relate the second steep conductivity decrease to the observed WL accompanying the elimination of the non-volatile carbonaceous residues, which takes place over the temperature range of ~ 420 to 550 °C (Fig. 1). Based on the TGA and *in situ* conductivity measurements, the PEG/MCM-41 composite was calcined at 550 °C for 3 h in air to eliminate the PEG molecules.

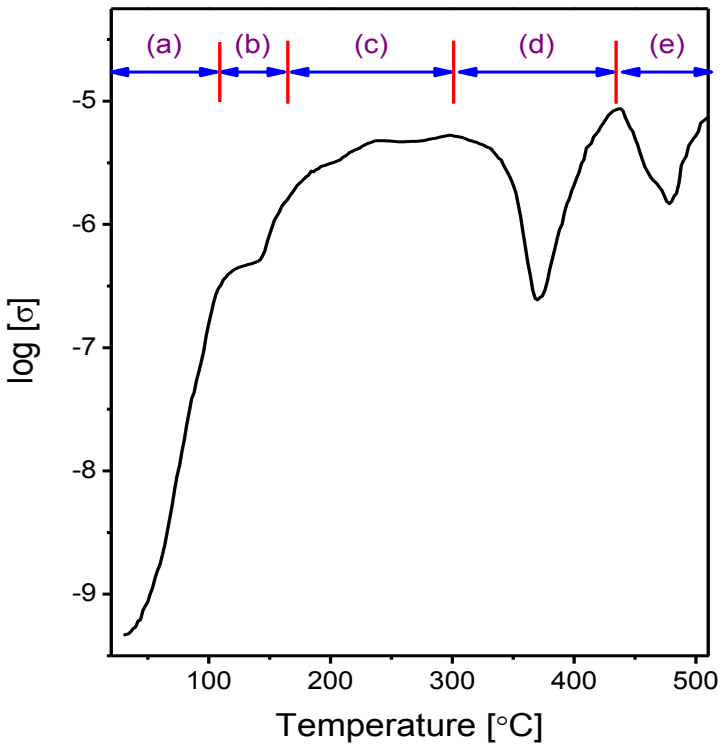

Figure 2. Plot of ln σ vs. temperature for MCM-41/PEG (25 wt. %) composite.

3.2 Characterization of the calcined PEG/MCM-41 composite

3.2.1 XRD and FT-IR analyses

X-ray diffraction patterns obtained for PEG/MCM-41 composite and its calcination product, formed in air at 550 °C, are shown in Fig. 3. Inspection of the low-angle XRD patterns (Fig. 3(A)) reveals that the composite shows a strong peak at the 2θ value of 2.8° due to the (1 0 0) diffraction of MCM-41 and a weak hump at 4-6.5°, which lies in the 2θ range of 3.8 to 4.8°, and a peak at 6.2-6.7° attributable to the higher order (1 1 0) and (2 0 0) diffractions of MCM-41 [21,22,26–29]. The relevant XRD pattern of the calcined sample reveals the existence of only one sharp peak at a 2θ value of 2.64°. No other peak exist in the 2θ range of 4 to 6.5°.

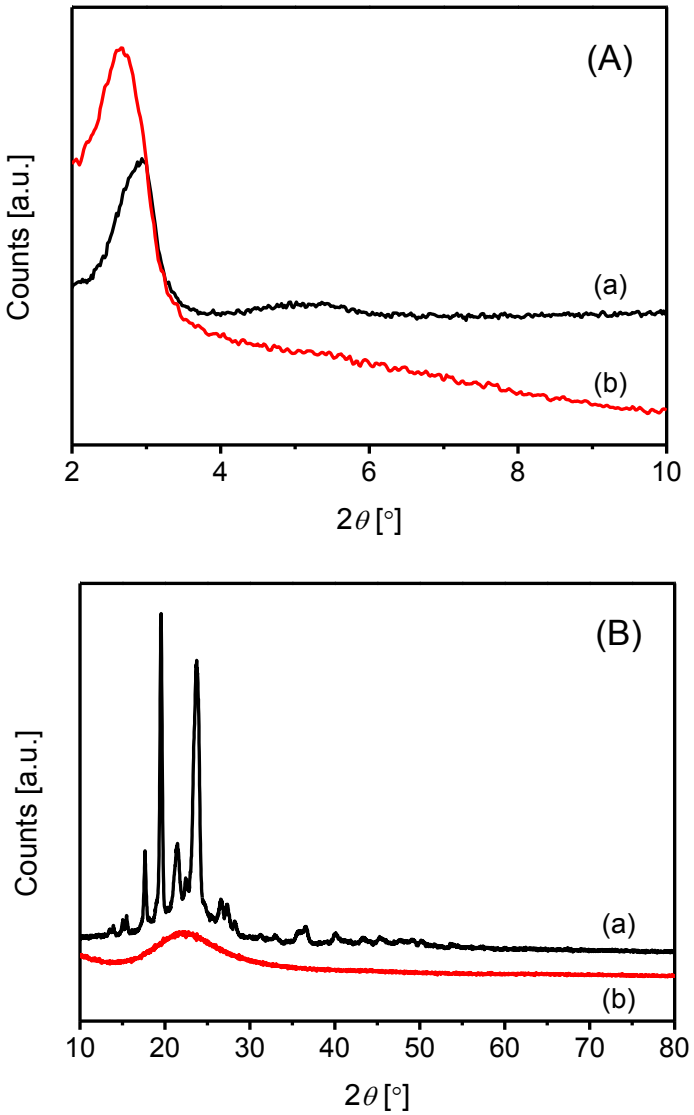

Figure 3. Low angle (A) and wide angel (B) XRD diffractograms of MCM-41/PEG 25 wt. % (a) and its 550 °C calcination product (b).

Several authors have reported a shift in the (1 0 0) reflection toward a higher 2θ value and a weakening or disappearance of other reflections characterizing the MCM-41 as a result of incorporation of metal cations or organic moieties into the MCM-41 matrix [23,26–28]. These modifications suggested that the mesoporous hexagonal symmetry was reduced by such treatments [23,26–28]. As a result, it seems plausible to suggest that the polymer evolution is not accompanied by a re-forming of the ordered MCM-41 structure. In other words, the calcined solid still exhibits the mesoporous MCM-41 framework with poor ordering.

At wider angles (Fig. 3(B)), the XRD pattern of the composite shows reflections due to the PEG [22,23]. The calcined sample, on the other hand, shows only the characteristic peak of amorphous silica with no appearance of any crystalline peak due to the PEG phase, suggesting the complete elimination of PEG from the silica framework of MCM-41.

Fig. 4 shows FT-IR spectra of the PEG/MCM-41 composite and its 550 °C calcination product. The FT-IR spectrum of the PEG/MCM-41 composite reveals the bands associated with both pure PEG and MCM-41. The spectrum obtained for the composite (Fig. 4(a)) reveals the presence of a broad band at approximately 3380-3450 cm^{-1}, which can be assigned to the stretching vibration of hydroxyl groups. The absorptions at 2889, 961, and 842 cm^{-1} can be attributed to the stretching vibration of the $–CH_2$ functional group, the crystal band of PEG and the C–C–O bonds, respectively [23,30,33,31]. The bands at 1152 and 1104 cm^{-1} are ascribed to the C–O–C stretching vibration. The bands located at 1104, 805 and 454 cm^{-1} can be assigned to the asymmetric $\nu_{Si–O}$, symmetric $\nu_{Si–O}$ and O–Si–O bending modes of MCM-41 [27,29,32–34]. The band at 964 cm^{-1} may be related to the stretching vibration of oxygen atoms not bridging two Si atoms resulting from Si–O- and Si–OH [33,34]. Therefore, the two bands at 1104 and 964 cm^{-1} can be related to both PEG and MCM-41. Calcining the composite at 550 °C resulted in a disappearance of the absorptions due to the PEG and the persistence of those ascribed to MCM-41 (Fig. 4(b).

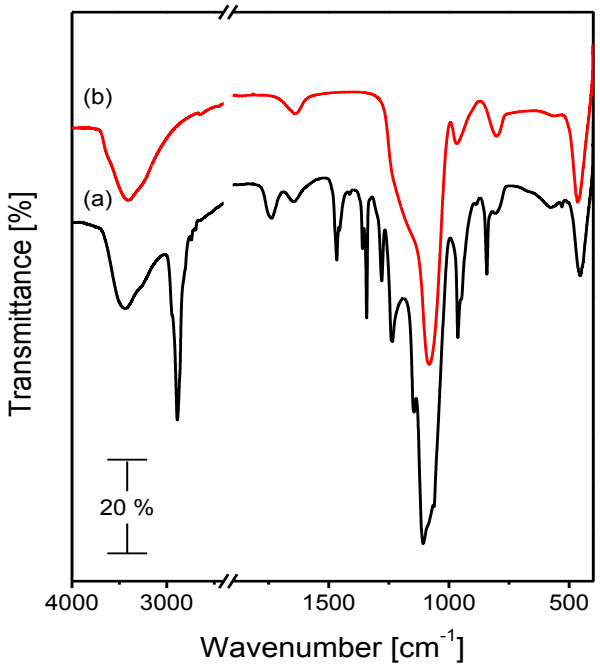

Figure 4. FT-IR spectra of MCM-41/PEG 25 wt. % (a) and its 550 °C calcination product (b).

3.2.2 Texture analysis and grain morphology

Figure 5(a) depicts nitrogen adsorption-desorption isotherms of pure MCM-41 and PEG/MCM-41 (25 wt. %) being calcined at 550 °C. The textural data obtained from the analysis of these isotherms are compiled in Table 1. Inspection of this figure reveals that the isotherm of MCM-41 belongs to the type-IV curves similar to those reported by many authors for meso-porous MCM-41 material [21,27–29,34–36]. Moreover, the desorption isotherm exhibits a type-H1 hysteresis loop. In the early stage of adsorption, the adsorption capacity increases gradually with an increase in P/P_o, in which the nitrogen molecules are adsorbed to the inner faces of the mesoporous materials. As the relative pressure increases, the isotherm reveals an inflection at approximately P/P_o = 0.3, which is due to capillary condensation within the meso-pores. Upon a further increase in P/P_o, the N_2 molecules are adsorbed onto the outer face of the meso-porous material, and the adsorptive capacity of the material increases slowly [21,27–29,34–36]. The amount of nitrogen adsorbed is lower for the calcined PEG/MCM-41 (25 wt. %) composite than for the neat MCM-41, which implies that it has a lower surface area. Moreover, the steepness after the inflection point is sharply decreased for the calcined PEG/MCM-41 sample. This indicates the loss of type-IV character of the MCM-41 after eliminating the PEG molecules. It is obvious from Table 1 that calcining the PEG / MCM-41 composite at 550 °C yields a sample with an S_{BET} value of 507 $m^2 g^{-1}$. This value is much lower than that of pure MCM-41 calcined at the same temperature (718 $m^2 g^{-1}$).

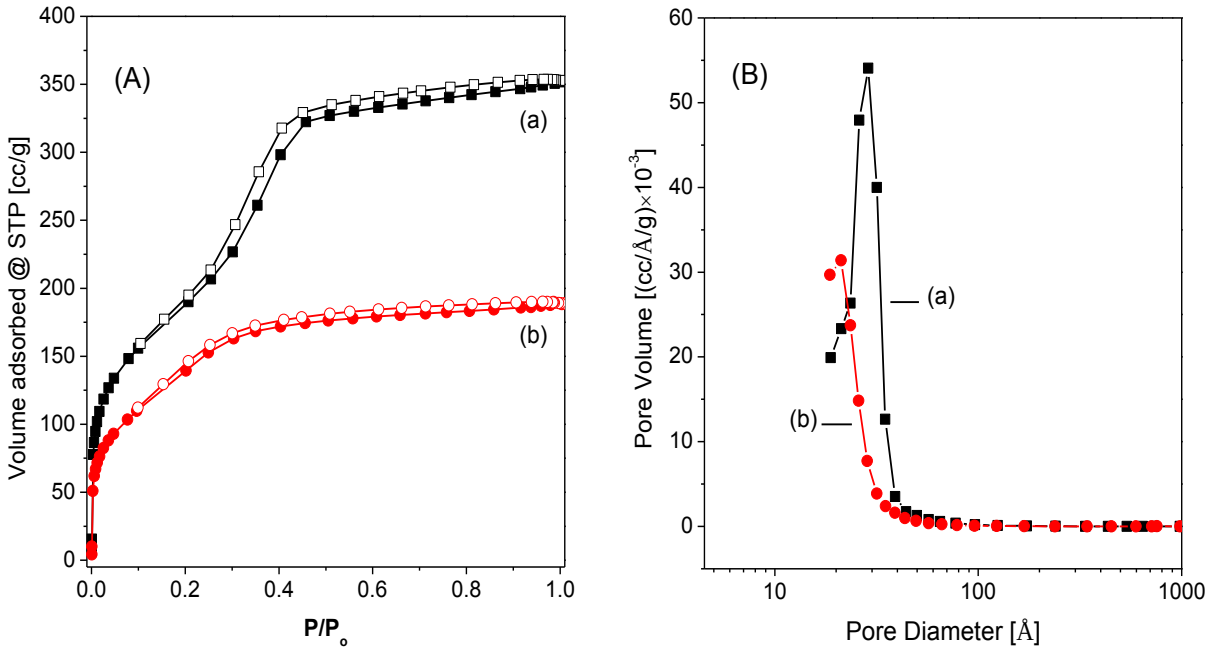

Figure 5. Nitrogen adsorption isotherms (A) and pore size distribution curves (B) of MCM-41/PEG 25 wt. % (a) and its 550 °C calcination product (b).

The pore size distribution curves of the calcined PEG/MCM-41 (25 wt. %) and pure MCM-41, calculated according to the BJH method from the desorption branches of the isotherms, are shown in Figure 5(b). The curve for MCM-41 shows one peak in the meso-porous region with a maximum

located at 28.7 Å. For the calcined PEG/MCM-41 sample, one can observe the presence of a shorter peak at 21.2 Å, which is located in the vicinity of the micro-porous region. From Table 1, it appears that the calcined MCM-41/PEG exhibits a smaller pore volume and smaller average pore diameter values. Pore narrowing should considerably decrease both the total pore volume and the pore diameters [37]. Thus, having a smaller pore volume and average pore diameter together with the observed shift in the meso-porous peak towards the microporous region (Figure 5(b)) indicates that the surface area decreases as a result of adding and then eliminating PEG molecules from MCM-41 material, which leads to a marked narrowing of the pores already present that have nearly the same dimension in the meso-porous range.

Table 1. Texture data obtained from the analysis of nitrogen sorption isotherms of the neat MCM-41 and MCM-41/PEG 30 wt. % composite being calcined at 550 °C.

Sample	S_{BET} [m^2/g]	External surface area [m^2/g]	Total pore volume [cc/g]	Average pore diameter [Å]
MCM-41 calcined at 550 °C	718	718	0.74429	29.149
MCM-41/PEG composite calcined at 550 °C	507	502	0.2916	23.346

The thermal analysis data demonstrated the elimination of PEG molecules upon heating the PEG/MCM-41 composites as high as 550 °C. The FE-SEM image of the calcined PEG/MCM-41 (25 wt. %) sample in Figure 6 illustrates that its morphology consists of uniformly dispersed globules. No structure related to the presence of PEG molecules was detected. This observation indicates that the loss of mesoporosity of MCM-41 as a result of polymer-matrix elimination is not accompanied by a noticeable change in the globular morphology that characterizes the MCM-41 material [22].

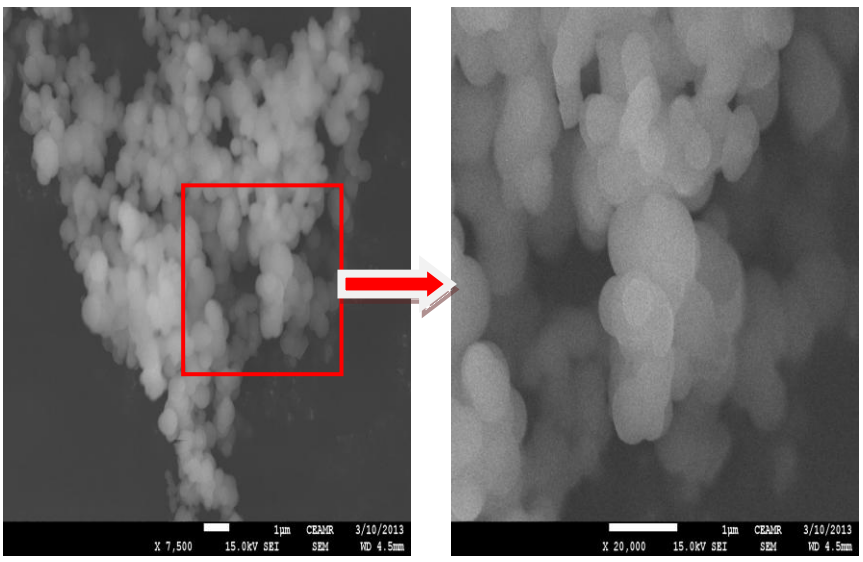

Figure 6. SEM images of the 550 °C calcination product of MCM-41/PEG 25 wt. %.

3.2.3 Electrical conductivity measurements

Measurements of the electrical conductivity were performed between 200 and 500 °C, in air, for MCM-41 and PEG/MCM-41 (25 wt. %) calcined at 550 °C. The activation energies of the conductance, E_σ, were calculated using the Arrhenius equation. Figure 7 shows the plots of ln σ versus the reciprocal absolute temperature for the two samples. Good linearity with the absence of inflection points was observed over the entire temperature range studied. Moreover, the conductivity values of MCM-41 are slightly higher than the corresponding values of the calcined PEG/MCM-41 composite. The calculated activation energies of conductance values for MCM-41 and the calcined composite are 116.13 and 108.34 kJ mol^{-1}, respectively. These values are in good agreement with those reported for zeolite-based materials [38,39]. The ion conduction in zeolites and zeolite-related structures is due to the migration of exchangeable cations, H^+ ions in our case, along the channels and cavities of the framework according to an ion-hopping mechanism [40]. The cation movement is controlled by: (i) the electrostatic interaction between the negatively charged framework and H^+ ions and (ii) the steric effects caused by the ratio of the size of the cations and the narrowest points in the channel system [39,40]. Sayler et al. [41] demonstrated that the electrical conductivity of the mesoporous silica monolith depends largely on the pore size and the mesopore interconnectivity within the monoliths. For porous MCM-type zirconium and titanium phosphates, it was reported that, although a partial contribution of the electronic conduction cannot be excluded, the major contribution must come from the proton mobility along the channels [42]. Recently, Sann et al. [43] reported a conductivity decrease of standard battery electrolytes in the presence of various mesoporous silicas (SBA-15, MCM-41 and KIT-6) with pores between 3 nm and 15 nm.

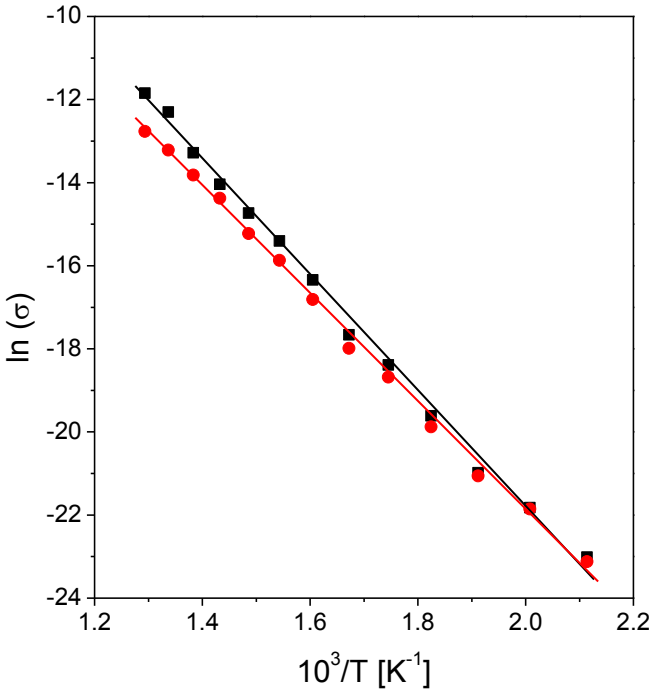

Figure 7. Plot of ln σ vs. the reciprocal of the absolute temperature for MCM-41 (■) and MCM-41/PEG (25 wt. %) composite (●) being calcined at 550 °C.

This decrease increases with silica mass fraction as well as with a decrease in the silica pore size. Based on this interesting literature data and bearing in mind the observed role of the pretreatment temperature in controlling the textural properties of the calcined composite, it is reasonable to suggest that the observed changes in the textural properties of the calcined composite plays an important role in hindering the movement of the charge carriers in the MCM-41. In other words the observed lower conductivity values can be correlated with the observed meso-porosity loss of MCM-41 material as a result of adding and then eliminating the PEG molecules.

4. CONCLUSIONS

In this investigation, a PEG/MCM-41 composite was prepared using a simple dissolution method. A mesoporous MCM-41 loading of 25% is used to form the targeted composite. TGA revealed that the thermal decomposition of the composite proceeds first with the loss of water molecules below 130 °C. The decomposition of the PEG molecules occurs in a steep step, maximized at 363 °C, which leaves a non-volatile carbonaceous residue that evolved in the temperature range of ~ 420 to 550 °C. I*n situ* electrical conductivity measurements demonstrated that the evolution of both the PEG and the carbonaceous residues is accompanied by an electrical conductivity decrease. Structural analysis of the calcined PEG/MCM-41 composite (at 550 °C for 3 h in air) proved that the elimination of PEG molecule results in a mesoporous MCM-41 framework with poor ordering. Nitrogen adsorption isotherms provided evidence for the textural modification of MCM-41 as a result of calcining the PEG/ MCM-41 (25 wt. %) at 550 °C. It was suggested that the elimination of PEG molecules is responsible for the observed surface area decrease as well as the mesoporosity loss. Moreover, it was found that the electrical conductivity was decreased for the 550 °C calcined composite compared with the neat MCM-41 calcined at 550 °C. This was attributed to the hindered mobility of the charge carriers as a result of the observed textural changes.

ACKNOWLEDGEMENTS
This work was funded by the Deanship of Scientific Research (DSR), King Abdulaziz University, Jeddah, under Grant No. (130-027-D1433). The authors, therefore, acknowledge with thanks DSR technical and financial support.

References

1. A.K. Geim and K.S. Novoselov, *Nat. Mater*., 6 (2007) 183.
2. G.W. Peng, F. Qiu, V.V. Ginzburg, D. Jasnow and A.C. Balazs, *Science*, 288 (2000) 1802.
3. T.C. Merkel, B.D. Freeman, R.J. Spontak, Z. He, I. Pinnau, P. Meakin and A.J. Hill, *Science*, 296 (2002) 519.
4. Y. Wang and N. Herron, *Science*, 273 (1996) 632.
5. N.S.M. El-Tayeb, B.F. Yousif and P.V. Brevern, In: Proceedings of the international conference on recent advances in mechanical & materials engineering, 30–31 May 2005, Kuala Lumpur, Malaysia; 2005. p. 1006.
6. N.S.M. El-Tayeb and B.F. Yousif, In: Proceedings of WTC2005 world tribology congress III September 12–16, 2005, Washington, DC, USA, Paper No. WTC 2005-63097.
7. K.L. Edwards, Mater. Des., 19 (1998) 1.
8. Saputra H, Othman R, Sutjipto AGE and Muhida *J. Membrane. Sci*., 367 (2011) 152.

9. C.T. Kresge, M.E. Leonowicz, W.J. Roth, J.C. Vartuli and J.S. Beck. *Nature*, 359 (1992) 710.
10. J.S. Beck, J.C. Vartuli, W.J. Roth, M.E. Leonowicz, C.T. Kresge, K.D. Schmitt, C.T.W. Chu, D.H. Olson and E.W. Sheppard, *J. Am. Chem. Soc*., 114 (1992) 10834.
11. J.M. Campos, J.P. Lourenco, E. Perez, M.L. Cerrada and M.R. Ribeiro, *J. Nanosci. Nanotechnol*., 9 (2009) 3966.
12. M.L. Cerrada, E. Perez, J.P. Lourenco, J.M. Campos and M.R. Ribeiro, Micropor. *Mesopor. Mater*., 130 (2010) 215.
13. N. Wang, Q.H. Fang, E.F. Chen, J. Zhang and Y.W. Shao, *Polym. Eng. Sci*., 49 (2009) 2459.
14. N. Wang, Y. Shao, Z.X. Shi, J. Zhang and H. Li, *J. Mater. Sci*., 43 (2008) 3683.
15. N. Wang, Z.X. Shi, J. Zhang and L. Wang, *J. Compos. Mater*., 42 (2008) 1151.
16. N. Wang, Q. Fang, Y. Shao and J. Zhang, *Mater. Sci. Eng*., A 512 (2009) 32.
17. N. Wang, Q. Fang, E. Chen, J. Shaohang and Y Shao, *J. Compos. Mater*., 44 (2010) 2083.
18. N. Wang, N. Gao, S. Jiang, Q. Fang and E Chen, *Compos*. B, 42 (2011) 1571.
19. N. Wang, Y. Shao, Z. Shi, J. Zhang and H. Li, *Mater. Sci. Eng*. A, 497 (2008) 363.
20. N. Wang, C.L. Zhao, Z.X. Shi, Y.W. Shao and H.W. Li, *Mater. Sci. Eng*. B, 157 (2009) 44.
21. M. Grün, K.K. Unger, A. Matsumoto and K. Tsutsumi, *Micropor. Mesopor. Mater*., 27 (1999) 207.
22. B.M. Abu-Zied, M.A. Hussein and A.M. Asiri, *Compos*. B, 58 (2014) 185.
23. B.M. Abu-Zied, M.A. Hussein and A.M. Asiri, *Polym. Compos*., 35 (2014) 1160.
24. S.A. Soliman and B.M. Abu-Zied, *Thermochim. Acta*, 491 (2009) 84.
25. B.M. Abu-Zied and S.A. Soliman, *Thermochim. Acta*, 470 (2008) 91.
26. S.G. Aspromonte, Á. Sastre, A.V. Boix, M.J. Cocero and E. Alonso, *Micropor. Mesopo. Mater*., 148 (2012) 53.
27. T. Lehmann, T. Wolff, C. Hamel, P. Veit and B. Garke, *Micropor. Mesopo. Mater*., 151 (2012) 113.
28. V.N. Jayaratne, S.L.Y. Chang, X. Fang and A.L. Chaffee, *Micropor. Mesopor. Mater*., 151 (2012) 466.
29. B. Li, K. Wu, T. Yuan, C. Han, J. Xu and X. Pang, *Micropor. Mesopor. Mater*., 151 (2012) 277.
30. W.L. Wang, X.X. Yang, Y.T. Fang and J. Ding, *Appl. Energy*, 86 (2009) 170.
31. W.L. Wang, X.X. Yang, Y.T. Fang, J. Ding and J.Y. Yan, *Appl. Energy*, 86 (2009) 1479.
32. X. Sheng, J. Gao, L. Han, Y. Jia and W. Sheng, *Micropor. Mesopor. Mater*., 143 (2011) 73.
33. S. Kiatphuengporn, M. Chareonpanich and J. Limtrakul, *Chem. Eng. J*., 240 (2014) 527.
34. R. Atchudan, A. Pandurangan and J. Joo, *Micropor. Mesopor. Mater*., 175 (2013) 161.
35. D.P. Liu, W.N.E. Cheo, Y.W.Y. Lim, A. Borgna, R. Lau and Y.H. Yang, *Catal. Today*, 154 (2010) 229.
36. X. Song, P. Qu, N. Jiang, H. Yang and G. Qiu, *Colloid Surf*. A, 313–314 (2008) 193.
37. N.E. Fouad, H. Knözinger, H.M. Ismail and M.I. Zaki, *Z. Phys. Chem*., 173 (1991) 201.
38. B.M. Abu-Zied, *Micropor. Mesopor. Mater*., 139 (2011) 59.
39. F.J. Jansen and R.A. Schoonheydt, *J. Chem. Soc. Farady. Trans*. 1, 69 (1973) 1338.
40. G. Kelemen and G. Schön, *J. Mater. Sc*i., 27 (1992) 6036.
41. F.M. Sayler, M.G. Bakker, J.H. Smatt and M. Linden, *J. Phys. Chem*. C, 114 (2010) 8710.
42. E. Rodríguez-Castellón, J. Jiménez-Jiménez, A. Jiménez-López, P. Maireles-Torres, J.R. Ramos-Barrado, D.J. Jones and J. Rozière, *Solid State Ionics*, 125 (1999) 407.
43. K. Sann, J. Roggenbuck, N. Krawczyk, H. Buschmann, B. Luerßen, M. Fröba and J. Janek, *Electrochim. Acta*, 60 (2012) 1.